Electronic Supplementary Material (ESI) for Physical Chemistry Chemical Physics.

Supplementary Information:

Direct spectroscopic evidence for the high-spin state of dioxidomanganese(v)

Olesya S. Ablyasova,[a,b] Vicente Zamudio-Bayer,[a] Max Flach,[a,b]
Mayara da Silva Santos,[a,b] J. Tobias Lau[a,b] and Konstantin Hirsch,*[a]

[a] *Abteilung für Hochempfindliche Röntgenspektroskopie, Helmholtz-Zentrum Berlin für Materialien und Energie, Albert-Einstein-Str. 15, 12489 Berlin, Germany.*

[b] *Physikalisches Institut, Albert-Ludwigs-Universität Freiburg, Hermann-Herder-Str. 3, 79104 Freiburg, Germany.*

∗ Corresponding author; e-mail: Konstantin.Hirsch@helmholtz-berlin.de.

S1 Crystal Field and Charge Transfer Multiplet Simulations of L-Edge XAS and XMCD Spectra of Dioxidomanganese(V)

The crystal field modifies the energies of the 3d orbitals and is implemented in CTM4XAS using the crystal field parameters $10D_q$, D_s, and D_t. The energy of the 3d orbitals in terms of the crystal field parameters is given by the following equations [1]:

$$E_{3d_{x^2-y^2}} = 6Dq + 2Ds - 1Dt \tag{S1}$$

$$E_{3d_{z^2}} = 6Dq - 2Ds - 6Dt \tag{S2}$$

$$E_{3d_{xy}} = -4Dq + 2Ds - 1Dt \tag{S3}$$

$$E_{3d_{xz,yz}} = -4Dq - 1Ds + 4Dt \tag{S4}$$

We start our simulations building on the electronic structure reported earlier in Ref. [2]. There are two occupied molecular orbitals in $[\mathrm{OMnO}]^+$ of $\mathrm{C_{2v}}$ symmetry that is $10\mathrm{a}_1$ and $4\mathrm{b}_1$ which simultaneously have considerable 3d character. In the main text of the paper we have shown that those are almost degenerate within 0.2 eV, while the molecular orbitals $2\mathrm{a}_2$, $11\mathrm{a}_1$, and $7\mathrm{b}_2$ remain unoccupied. The relation between the molecular orbitals and the 3d states is not unambiguous and the population of $10\mathrm{a}_1$ and $4\mathrm{b}_1$ can be either realized by a local 3d configuration of $3\mathrm{d}^1_{\mathrm{x^2-y^2}}$ $3\mathrm{d}^1_{\mathrm{xy}}$ or alternatively $3\mathrm{d}^1_{\mathrm{z^2}}$ $3\mathrm{d}^1_{\mathrm{xz}}$ depending on the choice of the frame of reference.

Please note that the implementation of the crystal field calculations in CTM4XAS will always result in degenerate $3\mathrm{d_{xz}}$ and $3\mathrm{d_{yz}}$ states, although this does not necessarily have to be the case in a molecule of $\mathrm{C_{2v}}$ symmetry. This allows us to devise three scenarios (combinations of fixed relations between crystal field parameters) that might be able to simulate the electronic structure reported in Ref. [2] and are shown in figure S1. The corresponding simulations of XAS and XMCD spectra for varying crystal field parameters are presented in figures S2 - S5.

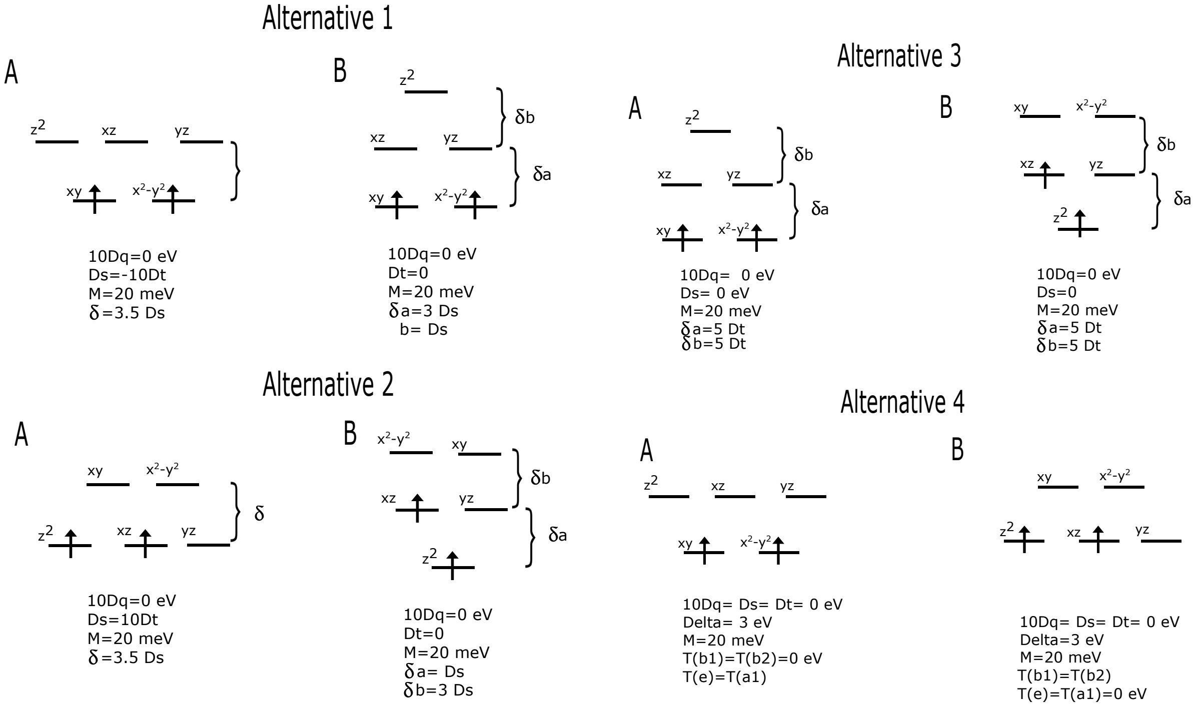

Figure S1: Both XAS and XMCD spectra of $OMnO^+$ are simulated employing a crystal field model. All possible level arrangements that are compatible with the ground state of $OMnO^+$ as reported in reference [2] are shown here as alternative 1-4.

Unfortunately, as can be seen from the figures varying the parameters in a wide range, none of those simulations can satisfactorily reproduce simultaneously the XAS and XMCD spectrum of $[OMnO]^+$. In figure S6 we also introduce a charge transfer, but again the agreement between simulation and experiment remains unsatisfactory.

Additionally, we use the relative energies of the molecular orbitals with significant 3d character extracted from the comparison of the oxygen K-edge spectrum and the oxygen p-projected density of states of $[OMnO]^+$ as described in the main text as input to crystal field simulations using the program package Xclaim [3]. Latter allows for shifting the energies of the individual 3d orbitals independent of symmetry considerations. Again the agreement with both XAS and XMCD signature is unsatisfactory as can be seen from figure S7.

Alternative 1 A

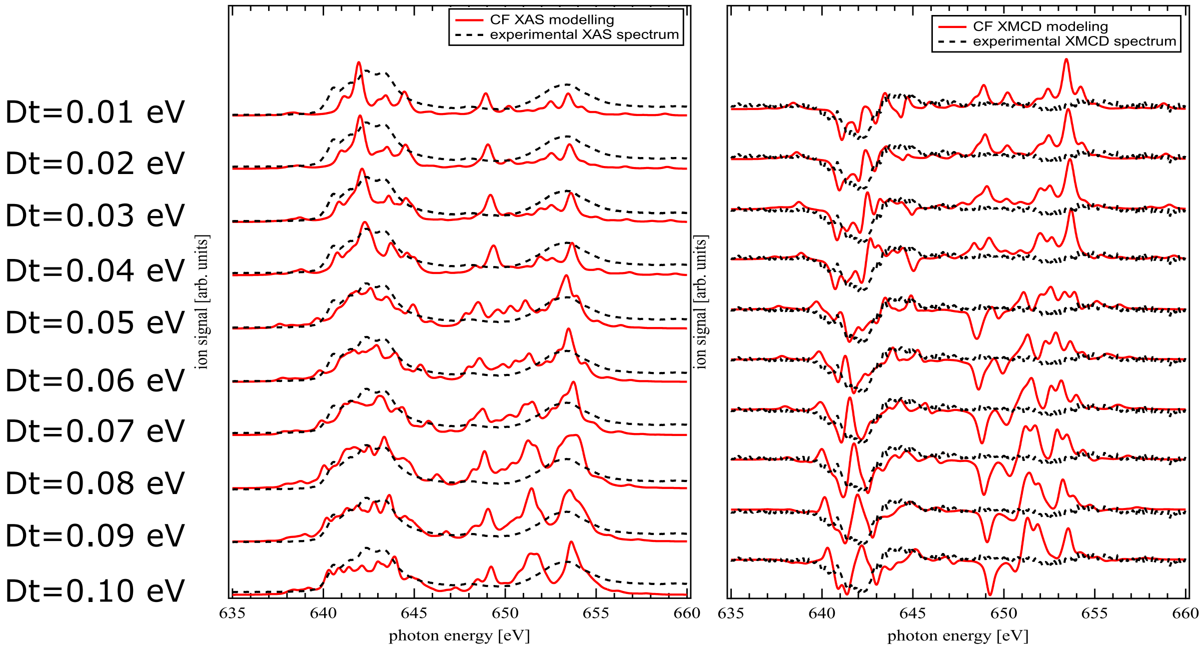

Alternative 1 B

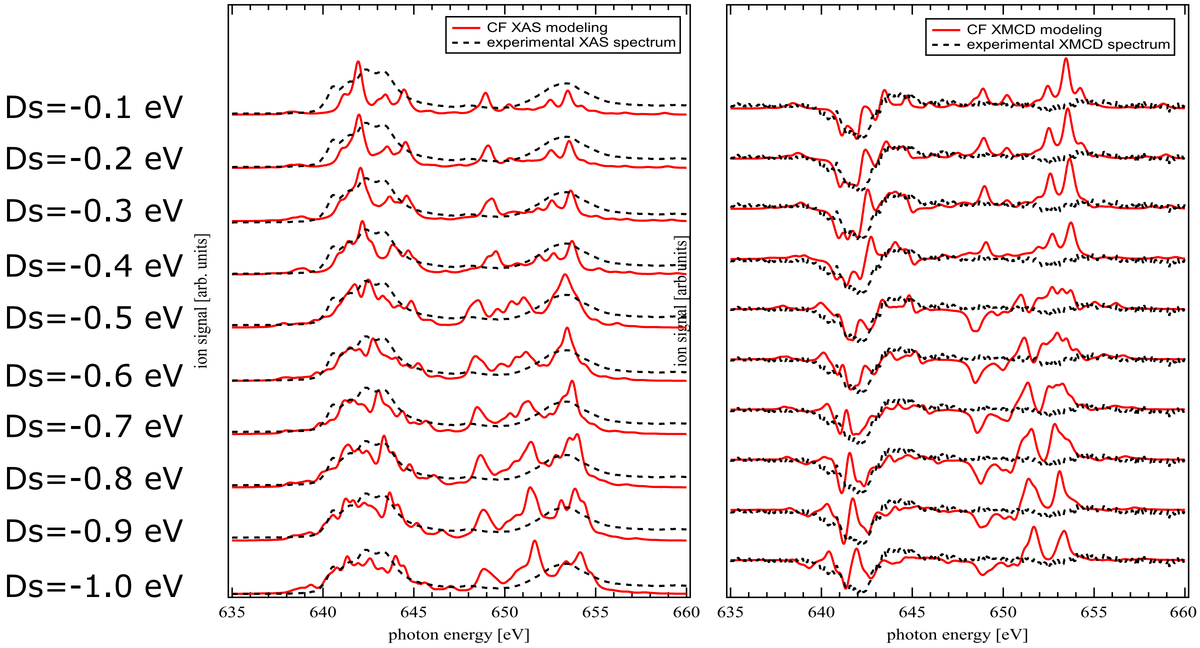

Figure S2: Crystal field simulations based on relative orbital energies as depicted in figure S1 resulting in simulated XAS (left panels) and XMCD spectra (right panels) compared to $[\mathrm{OMnO}]^+$ experimental spectra (dashed lines). Simulated spectra of both XAS and XMCD are shifted by -6.5 eV.

Alternative 2 A

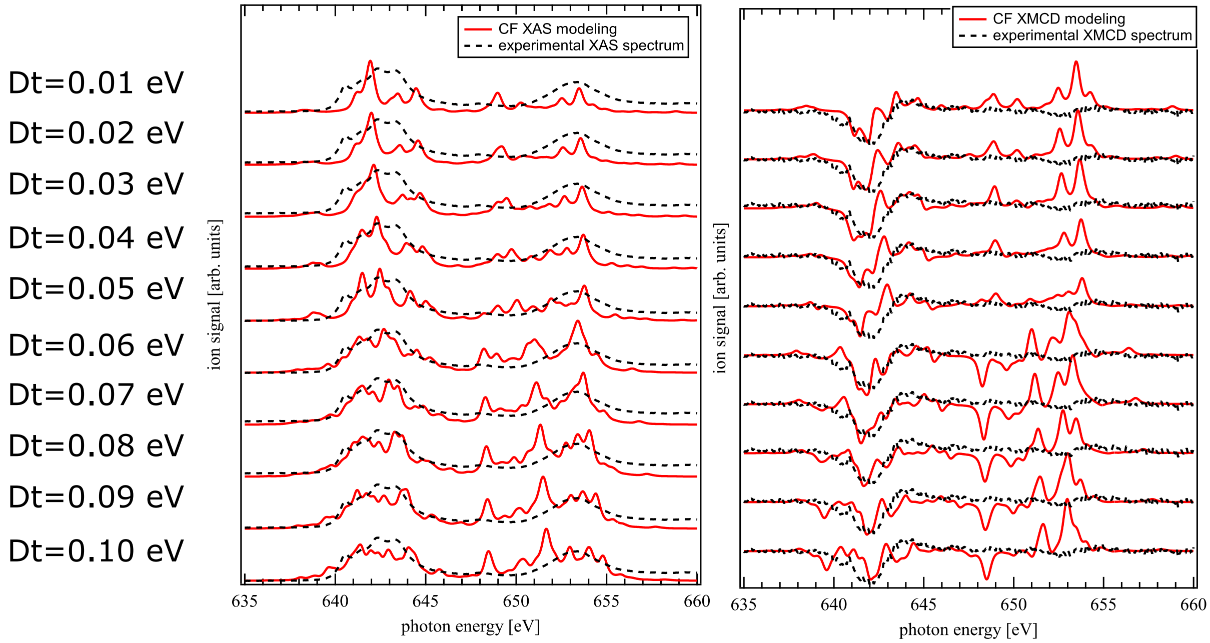

Alternative 2 B

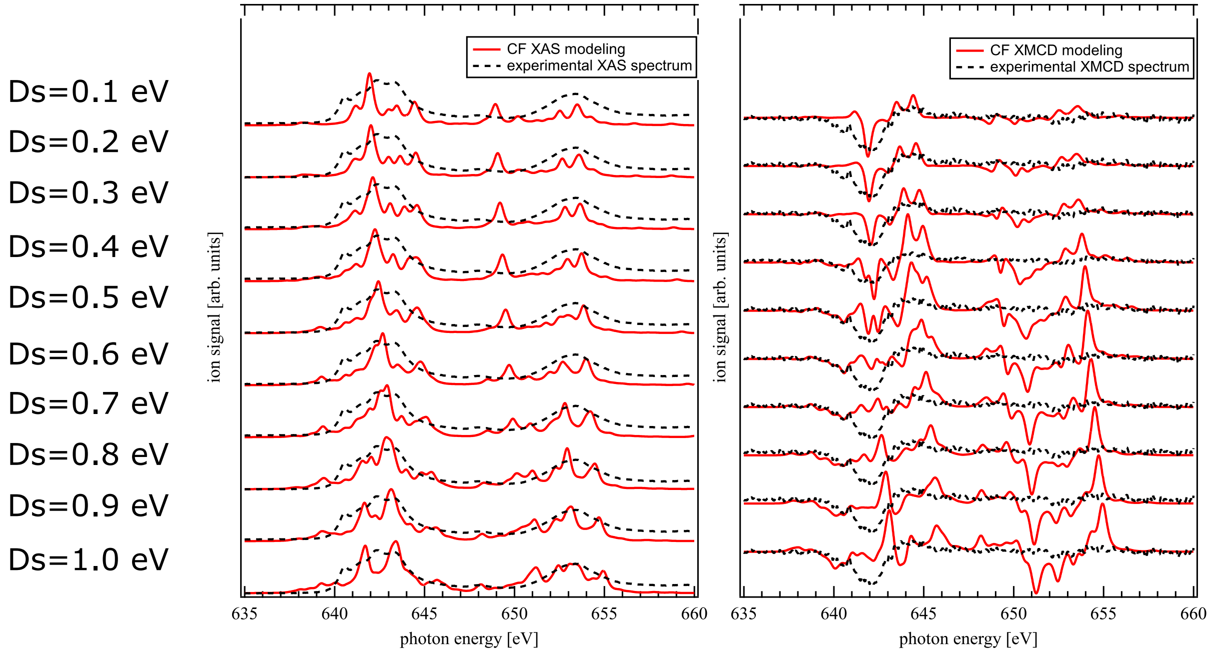

Figure S3: Crystal field simulations based on relative orbital energies as depicted in figure S1 resulting in simulated XAS (left panels) and XMCD spectra (right panels) compared to $[\mathrm{OMnO}]^+$ experimental spectra (dashed lines). Simulated spectra of both XAS and XMCD are shifted by -6.5 eV.

Alternative 3 A

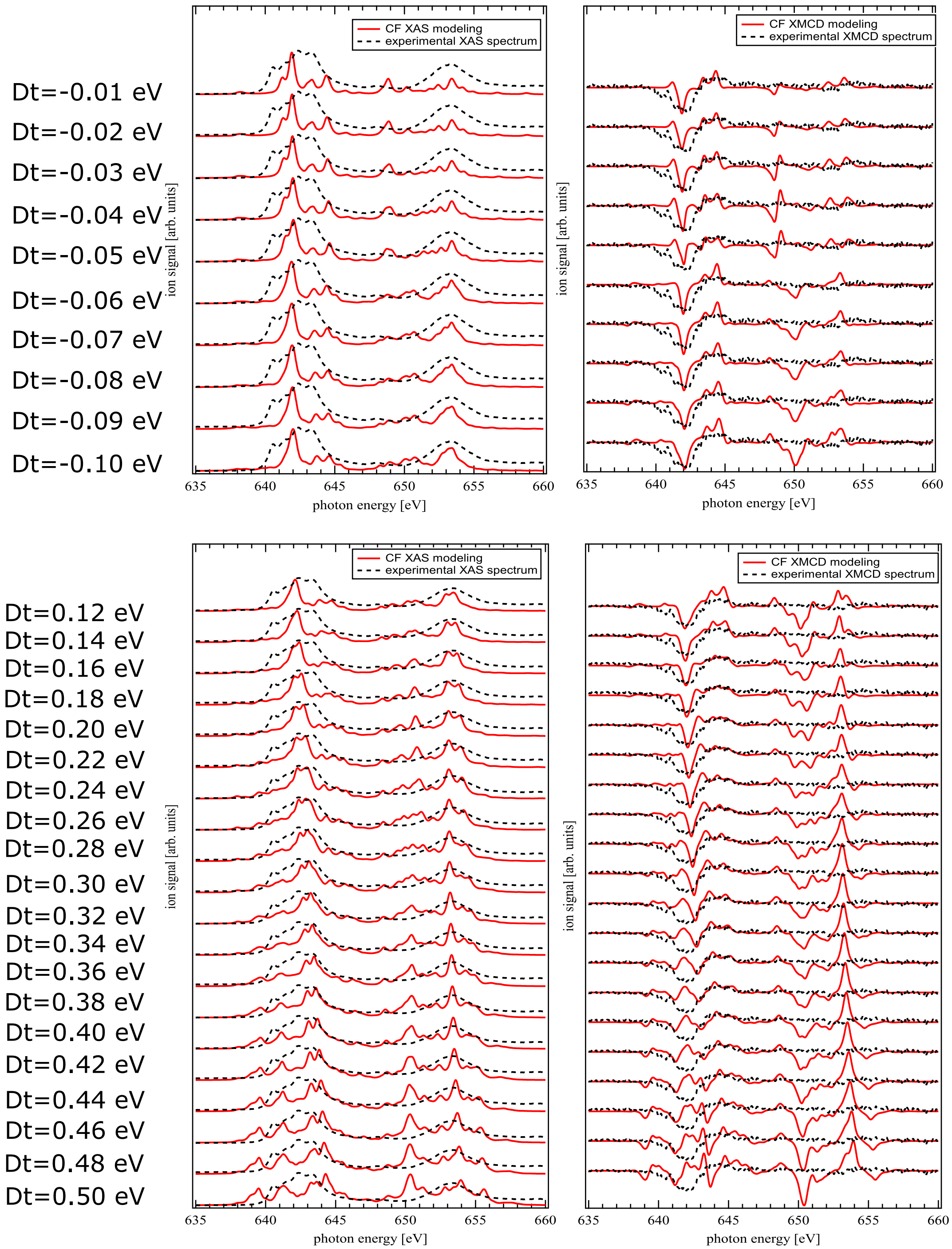

Figure S4: Crystal field simulations based on relative orbital energies as depicted in figure S1 resulting in simulated XAS (left panels) and XMCD spectra (right panels) compared to $[\mathrm{OMnO}]^+$ experimental spectra (dashed lines). Simulated spectra of both XAS and XMCD are shifted by -6.5 eV.

Alternative 3 B

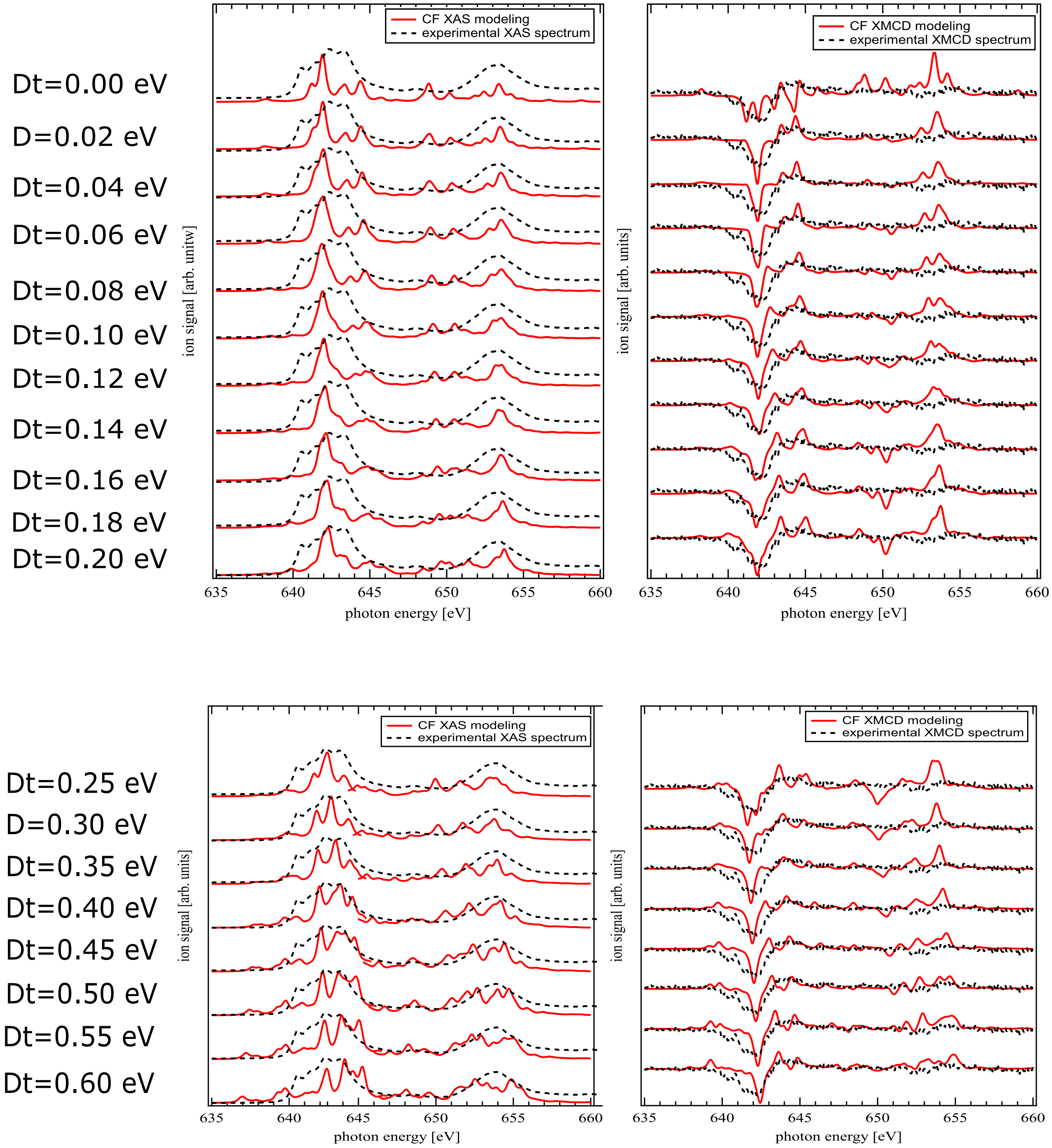

Figure S5: Crystal field simulations based on relative orbital energies as depicted in figure S1 resulting in simulated XAS (left panels) and XMCD spectra (right panels) compared to $[\mathrm{OMnO}]^+$ experimental spectra (dashed lines). Simulated spectra of both XAS and XMCD are shifted by -6.5 eV.

Alternative 4 A

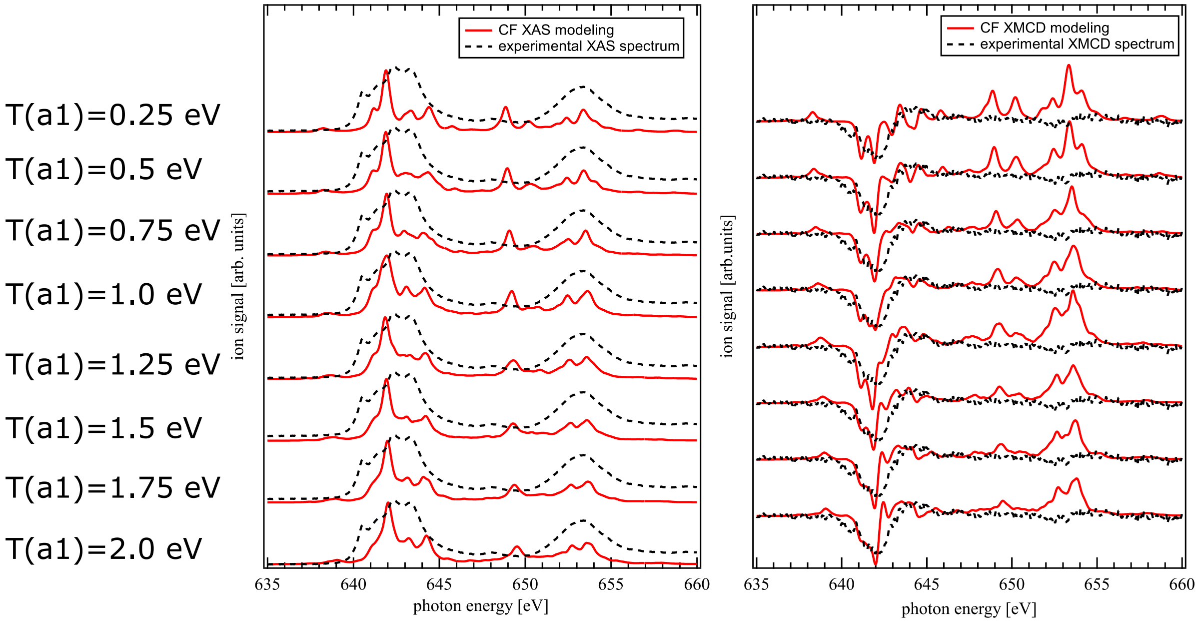

Alternative 4 B

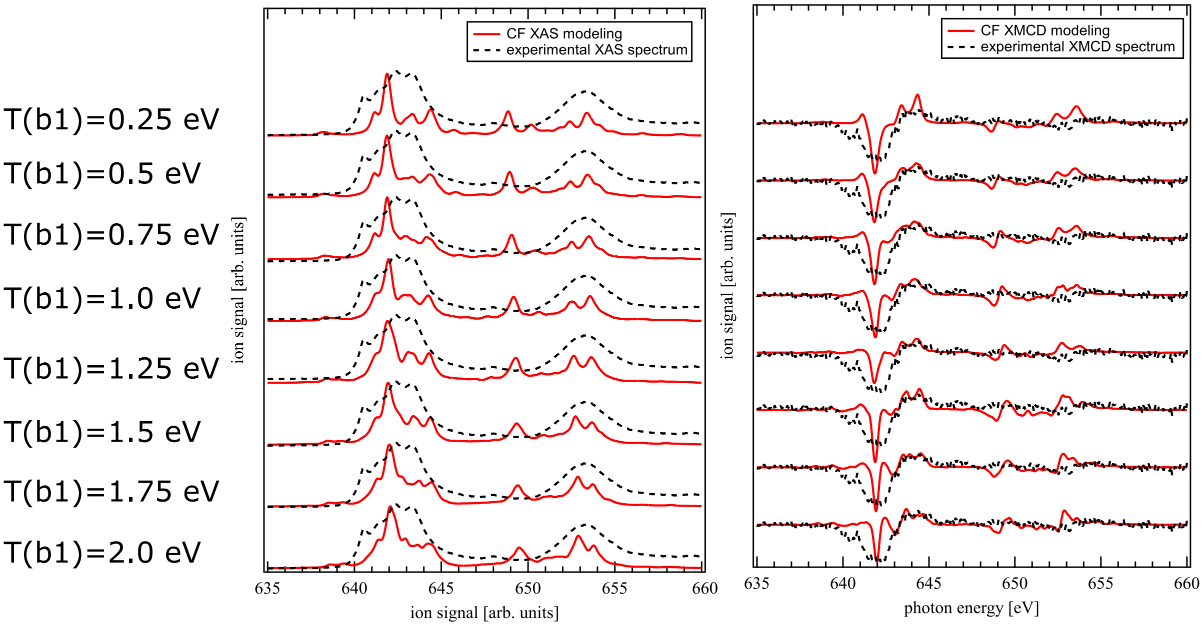

Figure S6: Charge transfer multiplet simulations using parameters as depicted in figure S1. The resulting simulations of XAS (left panels) and XMCD (right panels) are compared to the experimental data of $[\mathrm{OMnO}]^+$ (dashed lines). Simulated spectra of both XAS and XMCD are shifted by -6.5 eV.

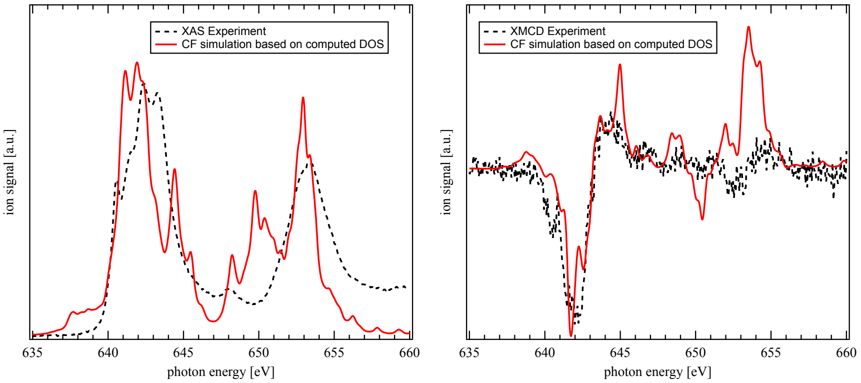

Figure S7: Comparison of experimental and crystal field simulations of XAS (left panel) and XMCD (right panel) based on the relative energies of the 3d states as derived from DFT calculations of $[\mathrm{OMnO}]^{+}$.

S2 Comparison of XAS and XMCD Spectral Signatures of $[\mathrm{OMnO}]^+$ with FeV_2O_4, VI_3 ($3d^2$) and CrI_3 ($3d^3$)

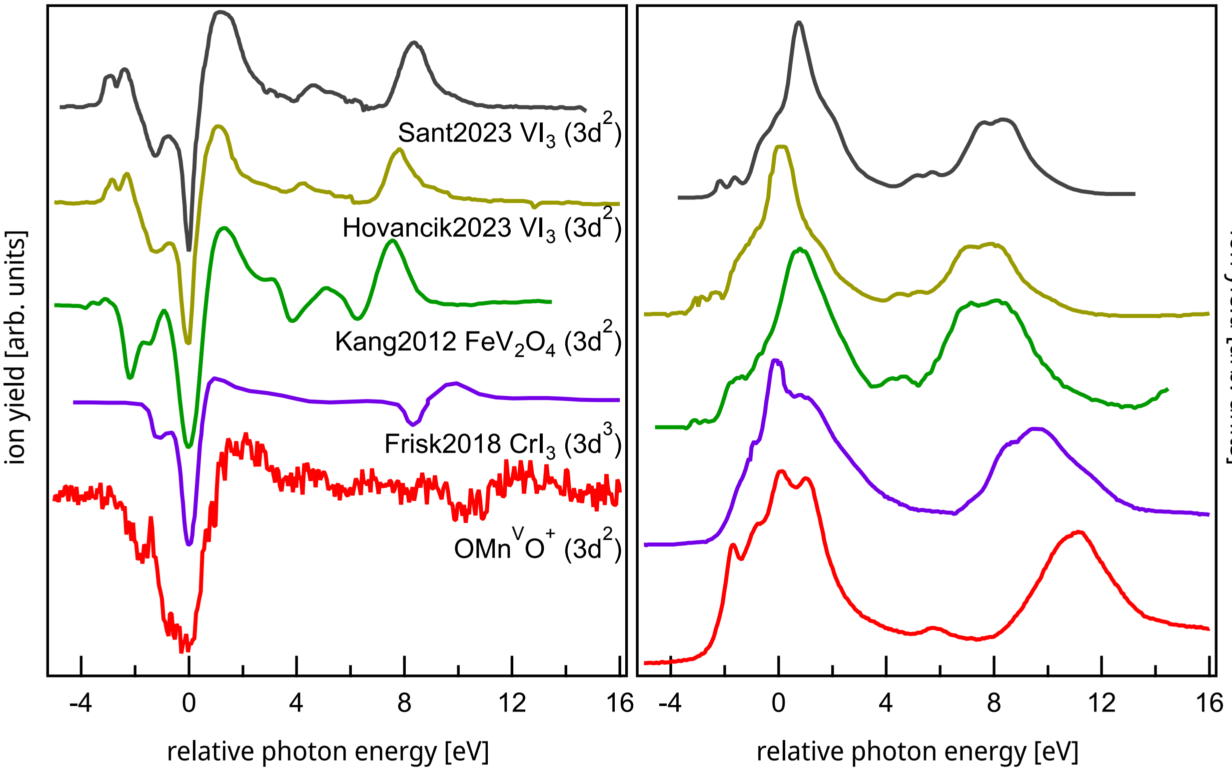

Figure S8: Comparison of XMCD (left panel) and XAS (right panel) signal at transition metal $L_{2,3}$ edges of $OMnO^+$ and other systems with local $3d^2$ [4, 5, 6] and $3d^3$ [7] electronic configurations. The spectra are shown on a relative photon energy axis as core level excitation energies of Mn, Cr and V differ by about 60 eV.

S3 Comparison of XAS and XMCD of $[\mathrm{OMnO}]^+$ and $[\mathrm{OMnOH}]^+$

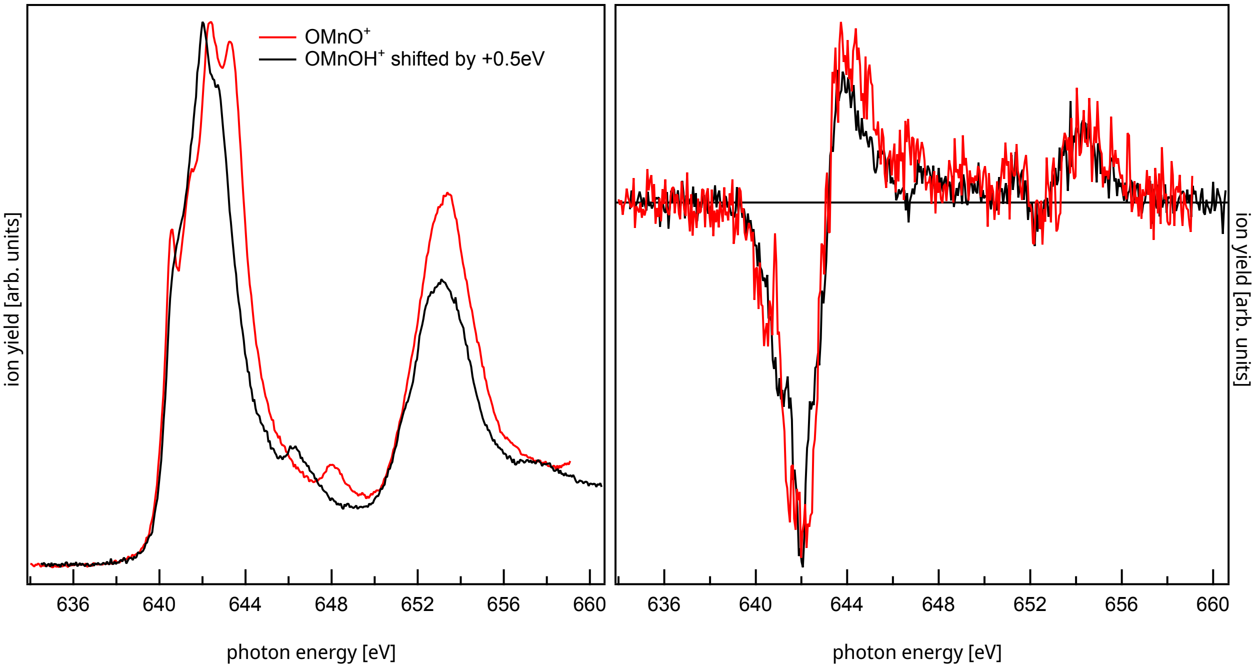

Figure S9: Comparison of manganese $L_{2,3}$ edge XAS (left panel) and XMCD (right panel) of $[\mathrm{OMnO}]^+$ and $[\mathrm{OMnOH}]^+$. The latter spectra are shifted in energy by 0.5 eV and scaled to match peak intensities of the spectra of $[\mathrm{OMnO}]^+$.

S4 Geometry Optimization and Electronic Ground State of $[\mathrm{OMnOH}]^+$ by DFT

We performed a search for the ground state geometry for $[\mathrm{OMnOH}]^+$ by starting from the known $[\mathrm{OMnO}]^+$ ground state structure [2] and placing the additional H atom either next to one of the oxygen atoms or the manganese metal center, respectively. Additionally we varied the multiplicity for all the starting geometries from 2 to 4 in agreement with the experimentally determined oxidation state. Furthermore, we varied the O-Mn-O bond angle in the starting geometry. The resulting structural motifs are presented in figures S10a-S10e. The geometry optimization has been performed using DFT employing the B3LYP functional [8, 9] along the def2-TZVP basis set [10] as implemented in the ORCA package version 4.2.1 [11]. The results are listed in table S1. The coordinates of the individual structures are given in section S7.

Table S1: Relative energies of isomers identified with structural motifs as presented in figures S10a-S10e alongside their spin multiplicity and structural parameters.

Relative Energy [eV]	Structural Motif	Multiplicity 2S+1	Mn–O bond distance [Å]	O–H bond distance [Å]	O–Mn–O bond angle [°]	O–O bond distance [Å]
0	1	4	1.603/1.699	0.973	123.5	2.916
0.67	1	2	1.515/1.684	0.972	144.7	3.050
2.26	2	4	2.144/3.202		12.5	1.203
3.17	4	2	1.530/1.530		114.8	2.577
3.86	2	2	2.099/3.165		12.4	1.203
4.10	3	2	2.245/2.241		31.6	1.221
5.48	5	2	1.669/3.114		28.7	1.835

(a) Structural Motif 1 (b) Structural Motif 2

(c) Structural Motif 3 (d) Structural Motif 4

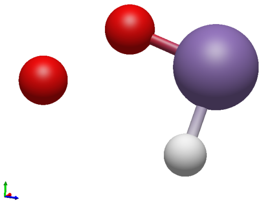

(e) Structural Motif 5

Figure S10: Calculated structural motifs for $[OMnOH]^+$

S5 Comparison of Mn $L_{2,3}$ and O K-edge of $[\mathrm{OMnO}]^+$ to Delcey et al.

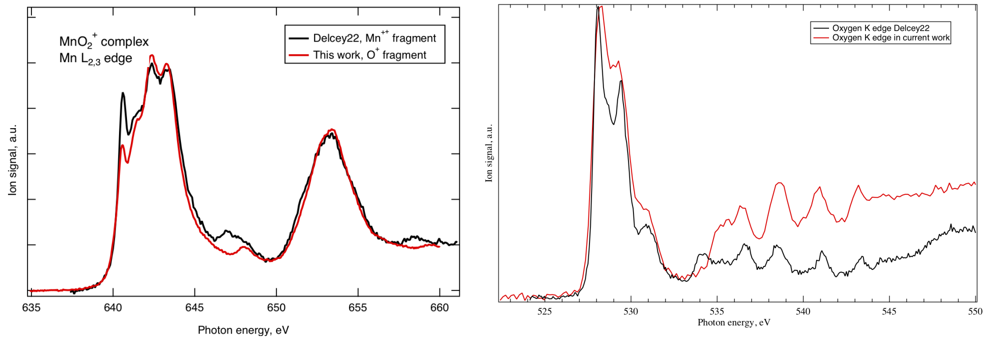

Figure S11: Comparison of the manganese $L_{2,3}$ edge (left side) and oxygen K edge (right side) of $[\mathrm{OMnO}]^+$ cluster, obtained by Delcey et al. [2] and the current work. Manganese $L_{2,3}$- and oxygen K-edge spectra were obtained from O^+ (this work) and Mn^{2+} (Delcey et al [2]) photo ion yield, respectively. This could explain some of the smaller differences between the spectra. Moreover, in the present work we took extra care of avoiding contamination by $[\mathrm{OMnOH}]^+$. The median position of the manganese L_3 edge is 642.6 ± 0.2 eV (this work) and 643 ± 0.3 eV (Delcey et al. [2]), respectively.

S6 Overview of Oxygen K-edge Spectra of $[\mathrm{OMnO}]^+$ and $[\mathrm{OMnOH}]^+$

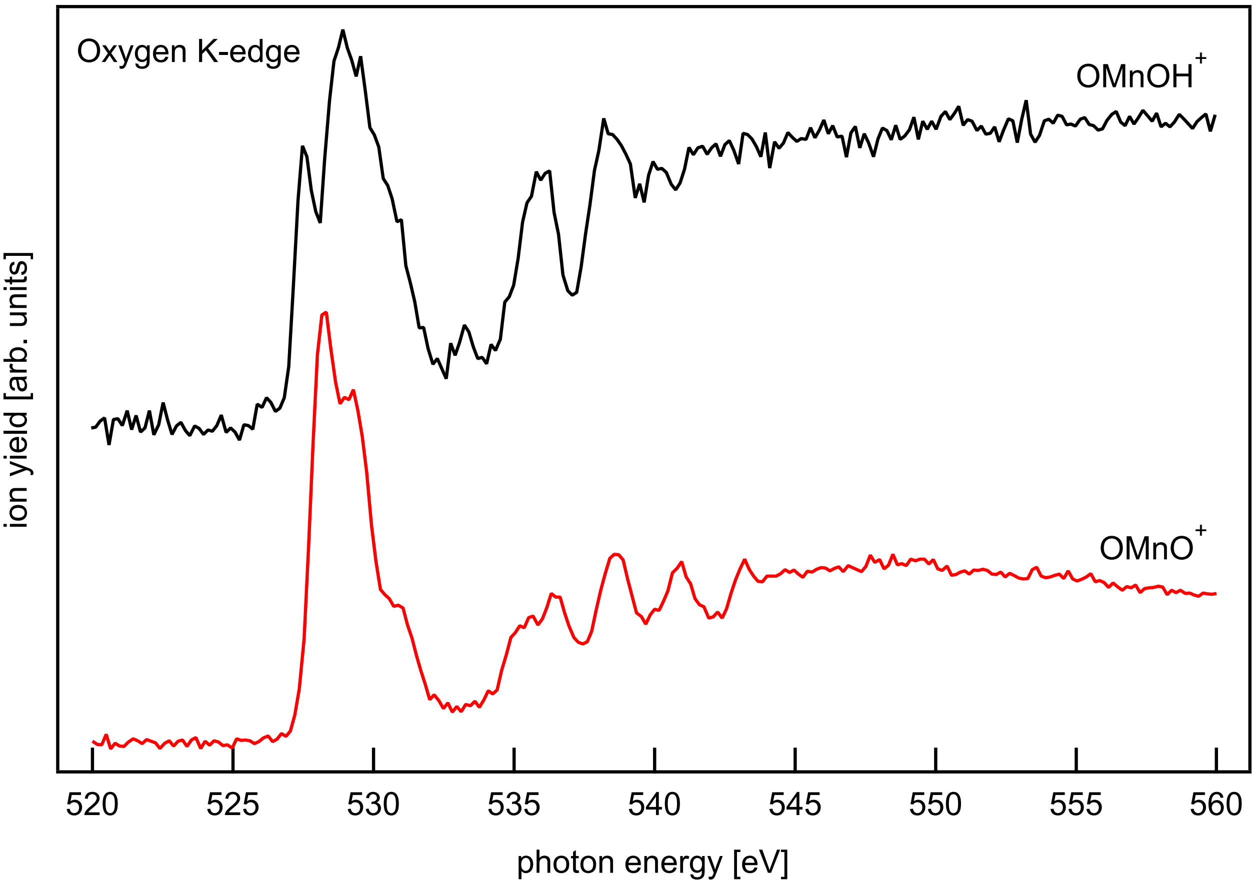

Figure S12: Oxygen K-edge overview spectra of $[\mathrm{OMnO}]^+$ and $[\mathrm{OMnOH}]^+$.

S7 Calculated Structures for $[OMnOH]^+$

Tabulated coordinates of the structures of cationic $[OMnOH]^+$ complex presented in SI table S1.

S7.1 Motif 1

S=2

element	x, Å	y, Å	z, Å
Mn	-0.0217090000	0.2798800000	0.3167180000
O	0.0305930000	1.7148620000	-0.1669740000
O	0.1188810000	-0.7225150000	1.6628010000
H	0.3020120000	-0.8257180000	2.6121740000

S=4

element	x, Å	y, Å	z, Å
Mn	-0.0695220000	0.1068620000	0.1749340000
O	0.0806760000	1.7009760000	0.0945640000
O	0.1066190000	-0.7813020000	1.6126760000
H	0.3120040000	-0.5800270000	2.5425450000

S7.2 Motif 2

S=2

element	x, Å	y, Å	z, Å
Mn	0.1827320000	0.4438440000	0.2741780000
O	0.4797650000	2.0438250000	-1.0518090000
O	1.1915270000	2.5062220000	-1.9042110000
H	0.4699940000	-0.9164000000	1.0082610000

S=4

element	x, Å	y, Å	z, Å
Mn	0.0989260000	0.4679060000	0.3174210000
O	0.4734030000	2.0666330000	-1.0619130000
O	1.2232350000	2.4775900000	-1.9078940000
H	0.5284530000	-0.9346390000	0.9788030000

S7.3 Motif 3

S=2

element	x, Å	y, Å	z, Å
Mn	0.4038810000	0.3576730000	-0.0169970000
O	0.1849470000	1.6666310000	-1.8273440000
O	1.0268250000	2.2034090000	-1.1238420000
H	0.2407010000	-0.7783690000	1.0622370000

S7.4 Motif 4

S=2

element	x, Å	y, Å	z, Å
Mn	0.4075270000	0.3027960000	0.1786570000
O	-0.0318150000	1.6599730000	-0.3742780000
O	-0.3431800000	-0.1517790000	1.4318520000
H	-0.4782620000	-0.4893370000	-0.7694940000

S7.5 Motif 5

S=2

element	x, Å	y, Å	z, Å
Mn	0.6166580000	0.9628840000	0.3801120000
O	-0.3255150000	0.5191990000	-2.5540760000
O	0.3762600000	1.5098680000	-1.1779480000
H	0.0537780000	-0.4863120000	0.1194310000

References

[1] Frank De Groot and Akio Kotani. *Core Level Spectroscopy of Solids*. CRC Press, Boca Raton, 2008.

[2] Mickaël G. Delcey, Rebecka Lindblad, Martin Timm, Christine Bülow, Vicente Zamudio-Bayer, Bernd von Issendorff, J. Tobias Lau, and Marcus Lundberg. Soft X-ray signatures of cationic manganese–oxo systems, including a high-spin manganese(V) complex. *Phys. Chem. Chem. Phys.*, 24(6):3598–3610, 2022.

[3] Javier Fernandez-Rodriguez, Brian Toby, and Michel Van Veenendaal. Xclaim: A graphical interface for the calculation of core-hole spectroscopies. *J. Electron. Spectrosc. Relat. Phenom.*, 202:81–88, 2015.

[4] J.-S. Kang, Jihoon Hwang, D. H. Kim, Eunsook Lee, W. C. Kim, C. S. Kim, Sangil Kwon, Soonchil Lee, J.-Y. Kim, T. Ueno, M. Sawada, Bongjae Kim, Beom Hyun Kim, and B. I. Min. Valence states and spin structure of spinel fev$_2$o$_4$ with different orbital degrees of freedom. *Phys. Rev. B*, 85:165136, Apr 2012.

[5] Dávid Hovančík, Jiří Pospíšil, Karel Carva, Vladimír Sechovský, and Cinthia Piamonteze. Large orbital magnetic moment in vi3. *Nano Letters*, 23:1175–1180, 2023.

[6] R. Sant, A. De Vita, V. Polewczyk, G. M. Pierantozzi, F. Mazzola, G. Vinai, G. van der Laan, G. Panaccione, and N. B. Brookes. Anisotropic hybridization probed by polarization dependent x-ray absorption spectroscopy in VI3 van der Waals Mott ferromagnet. *J. Phys.: Condens. Matter*, 35:405601, 2023.

[7] Andreas Frisk, Liam B. Duffy, Shilei Zhang, Gerrit van der Laan, and Thorsten Hesjedal. Magnetic X-ray spectroscopy of two-dimensional CrI3 layers. *Mater. Lett.*, 232:5–7, 2018.

[8] Axel D. Becke. Density-functional thermochemistry. III. The role of exact exchange. *J. Chem. Phys.*, 98:5648–5652, 1993.

[9] P. J. Stephens, F. J. Devlin, C. F. Chabalowski, and M. J. Frisch. Ab Initio Calculation of Vibrational Absorption and Circular Dichroism Spectra Using Density Functional Force Fields. *J. Phys. Chem.*, 98:11623–11627, 1994.

[10] Karin Eichkorn, Florian Weigend, Oliver Treutler, and Reinhart Ahlrichs. Auxiliary basis sets for main row atoms and transition metals and their use to approximate Coulomb potentials. *Theor. Chem. Acc.*, 97:119–124, 1997.

[11] Frank Neese. The orca program system. *WIREs Comput. Mol. Sci.*, 2:73–78, 2012.